

Discrete transverse superconducting modes in nano-cylinders

J. E. Han and Vincent H. Crespi

Department of Physics and Materials Research Institute,
The Pennsylvania State University, University Park, PA 16802-6300
(Dated: April 14, 2024)

Spatial variation in the superconducting order parameter becomes significant when the system is confined at dimensions well below the typical superconducting coherence length. Motivated by recent experimental success in growing single-crystal metallic nanorods, we study quantum confinement effects on superconductivity in a cylindrical nanowire in the clean limit. For large diameters, where the transverse level spacing is smaller than superconducting order parameter, the usual approximations of Ginzburg-Landau theory are recovered. However, under external magnetic field the order parameter develops a spatial variation much stronger than that predicted by Ginzburg-Landau theory, and gapless superconductivity is obtained above a certain field strength. At small diameters, the discrete nature of the transverse modes produces significant spatial variations in the order parameter with increased average magnitude and multiple shoulders in the magnetic response.

PACS numbers: 74.78.-w, 85.25.-j

I. INTRODUCTION

Recent developments in nanofabrication techniques allow access to new physical regimes where various intrinsic order parameters interact with a tuneable confining environment. Such order parameters cover an array of diverse physical systems, such as ferromagnets¹, quantum dots², molecular electronics³, photonic crystals⁴, superconductors^{5,6,7} etc. Quantum-confined superconductivity is particularly interesting for its macroscopic quantum nature; its well-understood microscopic mechanism can also serve as a platform for studies of other many-body nanoscopic quantum confinement effects.

Since the advent of BCS theory, a great deal has been understood in both the microscopic and phenomenological aspects of superconductivity for conventional phonon-mediated pairing systems. Theories have been immediately applied with great success to small superconductors^{7,8} of various geometry^{9,10}. Particularly useful has been the phenomenological Ginzburg-Landau theory, which describes superconductivity directly in terms of the superconducting order parameter without appealing to an underlying electronic basis.

Partly due to its enormous success, however, the Ginzburg-Landau theory has sometimes been applied beyond its strict regime of validity, especially in systems of small size. Part of the justification for this has been that experimental samples have often been disordered or polycrystalline, in which case confinement effects are less pronounced than they are for single crystals. Well-established dirty-limit theories for small superconductors with strong disorder¹¹ describe fascinating physics, such as gapless superconductivity, down to nanometer scales. In the clean limit of microscopic BCS theory, where the mean free path ℓ is longer than the coherence length ξ_0 ($\ell > \xi_0$), the superconducting behavior of small samples is very different from that in the dirty limit ($\ell < \xi_0$)^{10,12}. Recent experimental techniques for producing high quality single crystalline nanostructures

through electrodeposition into extended nanopores¹³ demands a re-examination of the phenomenology of superconductivity in such systems, working from microscopic theories. We specifically aim to investigate the often-overlooked spatial structures of the superconducting order parameter in the confined direction by directly solving the Bogoliubov-de Gennes equation and comparing with other theories.

For the last few decades, work on one-dimensional superconductivity has mostly focused on fluctuation effects^{14,15}. These treatments assume featureless transverse superconducting modes within superconducting nanowires and instead concentrate on the physics of phase slips in the axial direction. Here we complement these previous approaches by considering the effects of transverse quantum confinement on the spatial variation of superconducting order parameter, with consequences for the quasi-particle excitation spectrum and the magnetic response.

II. FORMALISM

We consider a superconducting cylinder with a radius R smaller than the penetration depth λ , but much larger than the atomic scale, so that we can describe the system with a continuum basis. The Bogoliubov-de Gennes (BdG) equations are

$$\begin{pmatrix} H_0 & u \\ H_0 & v \end{pmatrix} \begin{pmatrix} u \\ v \end{pmatrix} = E \begin{pmatrix} u \\ v \end{pmatrix} \quad (1)$$

where ψ is the order parameter and H_0 is the Hamiltonian for electrons,

$$H_0 = \frac{1}{2m} \left(\vec{p} - \frac{e}{c} \vec{A} \right)^2 + \mu_B H : \quad (2)$$

Here m is the band electron mass, μ_B is the chemical potential, \vec{A} is the Bohr magneton, σ is the Pauli spin

matrix and H is the external magnetic field. H_0 and its complex conjugate H_0^* act on the time-reversed electrons in Cooper pairs. The state $[u; v]$ represents the amplitudes of the pair of electrons which interact with each other via the pairing interaction parameterized by the superconducting order parameter Δ . For an axial magnetic field, $H = H \hat{z}$, the vector potential in the Coulomb gauge is:

$$A = \frac{1}{2} r H \hat{\phi}; \quad (3)$$

where $\hat{\phi}$ is an unit vector along the azimuthal direction. We assume that the radius of the nanorod is sufficiently below the penetration depth so that screening of the magnetic field due to demagnetization is negligible. In a cylindrical coordinate system H_0 becomes¹⁶:

$$H_0 = \frac{\hbar^2}{2m} \frac{\partial^2}{\partial r^2} + \frac{1}{r} \frac{\partial}{\partial r} + \frac{1}{r^2} \frac{\partial^2}{\partial \phi^2} + \frac{\partial^2}{\partial z^2} + \frac{1}{2} i \hbar \left(\frac{\partial}{\partial \phi} + \frac{1}{8} m \hbar^2 r^2 \right) B_z H \quad (4)$$

$$= K^0 + \frac{1}{2} \left(i \frac{\partial}{\partial \phi} - \frac{1}{8} m \hbar^2 r^2 \right); \quad (5)$$

where K^0 is the kinetic energy in zero external field (absorbing the chemical potential) and $\hbar \omega_c = e \hbar v_F / m c$ is the cyclotron frequency. With the typical separation of variables, the electron pair for the basis in Eq. (1) consists of time-reversed electrons in states (m, j, k) and $(-m, -j, -k)$ with m the azimuthal quantum number in $e^{im\phi}$ and k the z -wavevector in e^{ikz} . We explicitly write down the BdG equations by expanding $u(r)$ and $v(r)$ in terms of the eigenfunctions of K^0 as

$$u_{m,j}^k(r) = u_{m,j}^k(r) \frac{e^{im\phi}}{2} \frac{e^{ikz}}{L} \quad (6)$$

$$v_{m,j}^k(r) = v_{m,j}^k(r) \frac{e^{im\phi}}{2} \frac{e^{ikz}}{L}; \quad (7)$$

with L the length of the cylinder. We apply a boundary condition

$$u(r) = v(r) = 0 \text{ with } r = R; \quad (8)$$

so that the wavefunction vanishes outside the cylinder. This relation only imposes the condition that there are no electrons outside the cylinder and does not make any assumptions on the coarse-grained superconducting order parameters as usually treated in Ginzburg-Landau theory⁸. The radial term

$$m, j(r) = \frac{p}{2} \frac{J_m}{R J_{m+1}(p_{m,j})} \frac{r}{R}; \quad (9)$$

where J_m is the m -th order Bessel function and $p_{m,j}$ is its j -th zero. The operator K^0 is diagonal with matrix elements $K_{m,jk}^0 = \frac{\hbar^2}{2m} (p_{m,j}^2 + k^2)$. The BdG equation requires evaluation of matrix elements for \hbar^2 and

(r) . We will consider only the case of order parameters with zero net angular momentum and zero net momentum along z -axis, namely $m + m^0 = 0$ and $k + k^0 = 0$ in the product $u_{m,j}^k v_{m^0,j^0}^{k^0}$ for order parameter (r) . A paired state with finite net (angular) momentum has higher kinetic energy than the stationary solution, and is therefore disfavored¹⁷. With this choice of order parameter, we can compute the matrix elements for (r) and r^2 as

$$m, j, j^0 = \int_0^R \int_0^{2\pi} \int_0^L m, j(r) (r) m, j^0(r) r dr; \quad (10)$$

$$r_{m, j, j^0}^2 = \int_0^R \int_0^{2\pi} \int_0^L m, j(r) r^2 m, j^0(r) r dr; \quad (11)$$

The transverse modes (indexed with m, j) are decoupled from the longitudinal modes (indexed with k) and the gap equation is simplified.

The BdG equations Eq. (1) now become (with $I_{m, j, j^0} = \frac{1}{2} m, j, j^0$):

$$K_{m,jk}^0 \frac{1}{2} (m+1) \hbar^2 u_{m,j}^k + \sum_{j^0} \frac{1}{4} \hbar^2 I_{m, j, j^0} u_{m,j^0}^k + m, j, j^0 v_{m,j^0}^k = E_{m,j}^k u_{m,j}^k \quad (12)$$

$$K_{m,jk}^0 \frac{1}{2} (m+1) \hbar^2 v_{m,j}^k + \sum_{j^0} \frac{1}{4} \hbar^2 I_{m, j, j^0} v_{m,j^0}^k + m, j, j^0 u_{m,j^0}^k = E_{m,j}^k v_{m,j}^k \quad (13)$$

Note that the Zeeman term $\frac{1}{2} (m+1) \hbar^2$ have the same sign for $u_{m,j}^k$ and $v_{m,j}^k$ since they represent the amplitudes for time-reversed states. The order parameter (r) is self-consistently expressed by the typical gap equation

$$(r) = \frac{1}{V} \sum_{m,jk} [1 - 2f(E_{m,j}^k)] u_{m,j}^k(r) v_{m,j}^k(r); \quad (14)$$

where the summation range for the eigenstates is over kinetic energies $K_{m,jk}^0$ within a window $[-\hbar\omega_D; \hbar\omega_D]$ of width twice the Debye frequency $\hbar\omega_D$. We use generic parameter values suitable for conventional superconductors with T_c at few Kelvins. ω_D at $T = 0$ converges at large diameters as will be shown and we use the converged value $\omega_D = 3.9$ K as the bulk limit throughout this paper. m is set to the free electron mass, $\hbar\omega_D = 100$ K and $\omega_D = 10000$ K. As shown below, the Fermi velocity is then $v_F = 0.55 \times 10^8$ cm/sec and the coherence length $\xi_0 = \hbar v_F / \omega_D = 350$ nm in the bulk. Results are plotted in dimensionless units in this paper. Although we have chosen a particular set of parameters, we expect that our conclusion will hold qualitatively for conventional low- T_c superconductors.

As the diameter D ($= 2R$) shrinks, the transverse kinetic energy becomes very sensitive to the boundary condition, Eq. (8). Denoting a variation of radius R , $K^0 = K^0 + \delta K^0 = \frac{\hbar^2}{2m} R \delta R$. With a small uncertainty in radius $\delta R = 1$ Å around $R = 10$ nm, for example,

$K^0 = 0.02$ at 200 K , which is comparable to the Debye frequency. We incorporate the effects of variations in the wire diameter as a noise in the kinetic energy:

$$K_{mjk} = K_{mjk}^0 + s_{mjk} \frac{dK^0}{dR} R; \quad (15)$$

where s_{mjk} is a random number uniformly distributed in $[-1;1]$ and we set $R = 5\text{ \AA}$. Due to the time reversal symmetry of static scattering at the boundary, $s_{mjk} = s_{mjk}$. Here, we have partly taken into account the radial variations via energy levels, leaving unchanged the basis functions and the boundary condition. We have sampled equi-spaced z -momenta in the half Brillouine zone $[0; \pi]$ with 200–500 points, depending on the level of convergence required. Note that experimental nanowire samples to date have a significant variation in diameter along their length, but this variation is often slow on the length-scale of the nanowire width; the longest-wavelength variations could be subsumed into an adiabatic treatment.

III. RESULTS

The density of states of a nanorod can be expressed as the sum of one-dimensional densities of states $N_1(E)$ displaced by transverse energy eigenvalues E_\perp ,

$$N(E) = \sum_{\perp} N_1(E - E_\perp); \quad (16)$$

Quantized transverse levels strongly affect the density of states. Transverse modes are spaced with an average level spacing $E_\perp = 1/N_2$ with N_2 the 2-dimensional density of states, $N_2 = (R^2/m) (\pi \hbar^{-2})$. Since N_2 is independent of the chemical potential, the qualitative results do not depend on the particular position of the chemical potential. More details will be discussed in subsection IIIB. However, $N_1(E - E_\perp)$ has a van Hove singularity at $E = E_\perp$ and therefore small changes in the chemical potential can produce quantitatively different results. Concomitant effects become strong when the level spacing E_\perp is comparable to Δ , i.e.,

$$R \lesssim \frac{r}{m} \frac{\hbar^2}{\Delta}; \quad (17)$$

This condition becomes $D = 0.1$ with our parameters (and $\Delta = 3.8\text{ K}$). Due to the singularities in $N(E)$, solutions of the BdG equation are quite sensitive to model parameters for $D = 0.1$, even including a moderate smearing from R .

A. Large diameters

Superconductivity under confinement has been well studied for samples in the limit of $E_\perp \ll \Delta$ and D

$\gg \lambda_F$. For cylindrical samples with specular boundary conditions, we can explicitly solve Eq. (14) in the clean limit as a function of external magnetic field along the axis,

$$\ln(\alpha_0) = 1 + \frac{1}{2} \ln \frac{h}{2} + \frac{p}{2} \frac{1}{1} + \frac{3p}{2} \frac{1}{1^2}; \text{ for } > 1 \quad (18)$$

$$= 0; \text{ for } < 1$$

where $\alpha = h = \hbar$, $h = e v_F R \hbar = 2c$, and α_0 is the order parameter in bulk without external field. Strassler and Wyder¹² have obtained a result similar to the above equation for spherical systems and we follow essentially the same derivation for cylindrical systems in Appendix A. In this solution, we make a major assumption by ignoring the spatial variation of the order parameter, i.e.

$\psi(r) = \psi_0$. In carrying out an analytic calculation from Eq. (14), we make further approximations that the position and momentum in Eq. (14) commute and that the terms quadratic in the field $\frac{1}{4} m \hbar^2 I_{mjk}$ in Eq. (13) are negligible. When compared with a numerical solution of the full BdG equations, the above approximations seem reasonable in the large D regime for zero external magnetic field, (until $D = 0.57$ for our parameter values).

This clean-limit solution has a field dependence quite different from the standard Ginzburg-Landau prediction. Instead of gradually decaying from the zero-field order parameter α_0 to zero, α stays constant up to $H_1 = 2c_0 = e v_F R$ and then drops to zero at the critical field H_c , (see solid line in Fig. 1)

$$H_c = \frac{1}{2} \exp(3/2) H_1 = 0.454 \frac{c_0}{R}; \quad (19)$$

with the flux quantum $\phi_0 = hc/2e$ and the coherence length $\xi_0 = \hbar v_F / \Delta$. The critical field depends inversely on the diameter, since orbital motions of electron in small samples are less influenced by magnetic field. H in Fig. 1 is defined as H_1 for $R = \xi_0$, i.e., $H = 2c_0 = e v_F \xi_0$.

We have solved the BdG equations under two different conditions: first with the constraint of a spatially uniform order parameter and then with the constraint relaxed. The quantitative results and their overall line shapes (in Fig. 1) are in good agreement with the analytic formula Eq. (18). First comparing the analytic result with the uniform calculation, we find that the invariant order parameter up to $H = H_1$ is well reproduced. The numerical deviates downward from the analytical formula at higher values of H , resulting in smaller critical field H_c . We attribute the discrepancy to underestimation of the external field in the analytic solution due to ignoring the A^2 term. Further discussion is given at the end of this subsection.

An important qualitative deviation of the full BdG solution from the uniform results comes at high fields near H_c . The critical field for the full BdG solution (solid

circles in Fig. 1) extends to high elds, with decaying much slower than the usual square-root drop¹⁹ of the uniform solution. It is clear that this phenomenon must originate from the transverse spatial variation of the order parameter, which we will discuss below in more detail.

Although the average order parameter remains constant for $0 < H < H_1$ (left to the dashed line in Fig. 1), the density of states reveals a closing of the excitation gap at the eld H_1 (dashed curve in Fig. 2), where the spectral weight at the chemical potential becomes finite. The density of states in the gapped region continues to increase until $H = H_c$. In the clean limit, the electron trajectories are not perturbed by impurity scattering and their angular momentum L couples to the external eld as $(e=2m_c)L = H$. This coupling gives the term $\frac{1}{2}m \sim \frac{1}{2}c$ in Eq. (13) and contributes to the quasi-particle excitation energy E_{mj}^k ,

$$E_{mj}^k = \frac{q}{K_{mj}^0} \sqrt{2 + \frac{1}{2}(m+1)\hbar c} \quad (20)$$

These angular momentum contributions dominate over spin contributions and the excitation spectrum goes gapless when $(e=2m_c)\hbar L = H$ i.e. $HR = 2c$. In contrast, when impurity scattering dominates, the electron trajectories are disrupted and the quasi-particle energy is no longer in the form of Eq. (20). In this limit, the quasi-particle energy suffers significant level broadening and experiences shifts only from the spin Zeeman term²⁰. Therefore, away from the clean limit the density of states retains the form of a conventional gapped superconductor¹².

At zero eld, the order parameter is nearly constant over the cylinder (see Fig. 3), except for small oscillations and a Gibbs's phenomenon at $r = R$. The rapid oscillations have a wavelength proportional to $1/v_F$ and an amplitude that diminishes for larger diameters. Therefore we expect that these oscillations will be averaged out on larger length scales; they are not important for large-diameter systems. In such regime, we correctly reproduce the boundary condition commonly used in the literature, namely a vanishing normal derivatives of the superconducting order parameter at the surface. The order parameter does not change until $H = H_1$. As H exceeds H_1 , some quasi-particle energies are pushed below zero in Eq. (20) and contributions from these excited quasi-particle states reduce the order parameter in Eq. (14) by changing the signs of their contributions in the statistics factor, $1 - 2f(E_{mj}^k)$. In addition to an overall reduction of $\langle r \rangle$ under external eld, $\langle r \rangle$ also changes slope, with a distinct knee that moves towards $r = 0$ with increasing eld (see arrows in Fig. 3). At a radius r , the angular momentum is of order $m \sim rv_F$ and the order parameter begins to be suppressed when $m \sim rv_F \hbar = 2c$ or $r \sim 2c / (ev_F \hbar)$. This simple argument should be taken with caution, since the semi-classical approximation of treating position and momentum as commutable in Eq. (14) becomes worse when there is a strong spa-

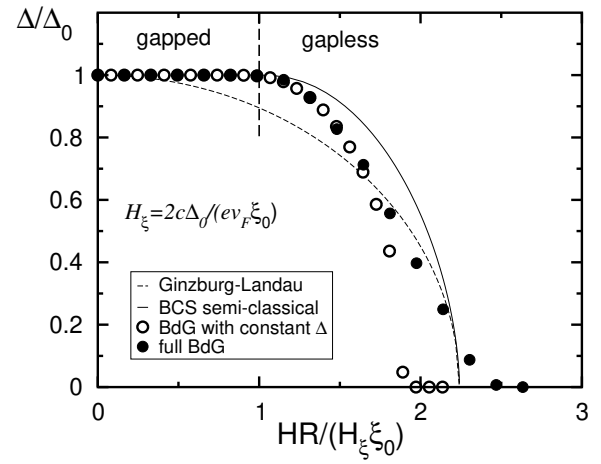


FIG. 1: Averaged superconducting order parameter in a cylindrical sample of large diameter ($D = 200 \text{ nm}$, $D/D_0 = 0.57$) with axial external magnetic elds. Normalized order parameter to the zero eld value Δ_0 is plotted as a function of dimensionless eld $HR = (H/H_0)$ with $H_0 = 2c/\xi_0 = (ev_F \hbar)$. Overall agreement of the analytic formula Eq. (18) and the numerical results are good. Solution of Bogoliubov-de Gennes (BdG) equation in the clean limit remains constant until $H_1 = 2c/\xi_0 = ev_F \hbar$. Full solution of the BdG equation (solid circles) has larger order parameters near the critical eld than those constrained to a spatially uniform (open circle) due to

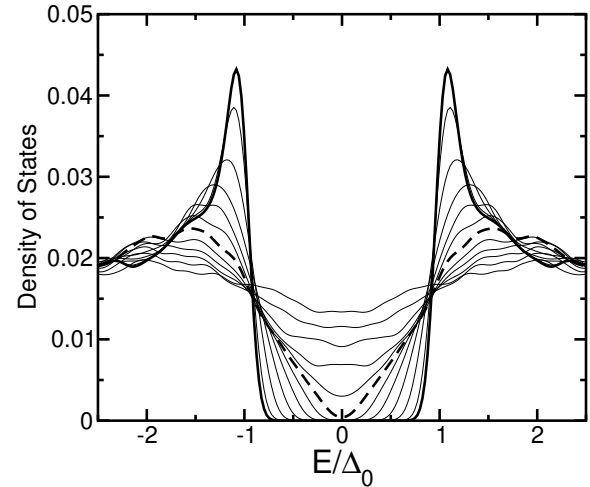


FIG. 2: Density of states as a function of external eld. Superconductor becomes gapless at $H = H_1$ (dashed line) in the clean limit well before the critical eld H_c , due to the coupling of orbital angular momenta to external eld. The external elds in the plot are from $HR = (H/H_0) = 0$ (thick line) to 1.83 with equal intervals between the curves.

tial variation.²¹ At larger radius r , the energy difference between the angular momenta (with $m \sim m \sim rv_F$) in an electron pair exceeds the pairing energy and therefore the pair becomes depaired.

We emphasize that the pronounced radial dependence of order parameter is related to the coupling of orbital

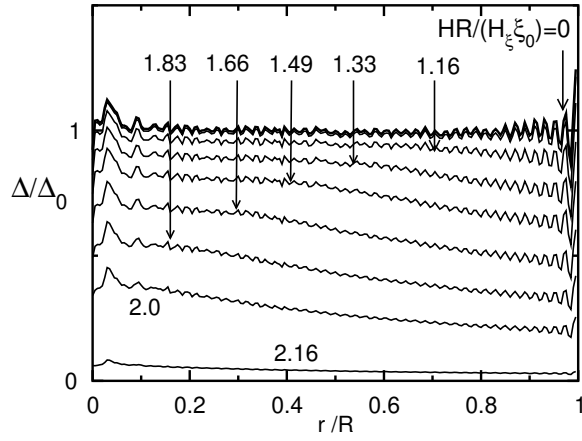


FIG. 3: Spatial variation of order parameter in the large diameter limit ($D = 0 = 0.57$). For external fields of $0 < H < H_1$, remains at A . As the field increases from H_1 , drops with a knee which progresses towards $r = 0$.

angular momentum to the external field, rather than the term $\frac{1}{8}m^2 r^2$ in Eq. (5), which makes the superconducting order parameter more massive. To compare these two contributions, we consider the Ginzburg-Landau theory with an order parameter of zero total angular momentum, as is usual in the literature^{7,8}; (see appendix B). The order parameter couples to the external field only through $\frac{1}{8}m^2 r^2$ and does not have any information about the angular momentum of constituent electrons in Cooper pairs. The spatial dependence of $\Delta(r)$ arising from the term $(2e\hbar c)^2 A^2$ turns out to be much weaker than the angular momentum coupling in the BdG treatment. The resulting critical field Eq. (B5) is almost identical to the angular momentum depairing result Eq. (19), as both are derived in detail in the appendix.

It is interesting to note that, although the orbital coupling and the A^2 -coupling produce very close critical fields (see Eqs. (19, B5)) in the absence of the other, they do not act additively when both are present. When the A^2 -term is included on top of the orbital coupling, its effect becomes significantly smaller than in Eq. (B5) because the orbital effect produces fast-decaying $j(r)j^2$ near $H = H_c$. For example, the curve labeled with $HR/(H_c \xi_0) = 2.16$ in Fig. 3 has $j(r=R)j^2 = j(r=0)j^2 = 1/7$. Since the $A^2 = H^2 r^2$ term couples most strongly at large r , the actual $A(r)^2 j(r)j^2$ coupling is much smaller than the Ginzburg-Landau theory. For instance, a reduction of the effective A^2 -coupling by half results in the reduction of the order parameter by $1/(1+0.5) = 82\%$ in terms of the Ginzburg-Landau theory when the both couplings are naively added, which nearly matches the discrepancy in Fig. 1 between the Eq. (18) (thin line) and the constant- (open circles) results.

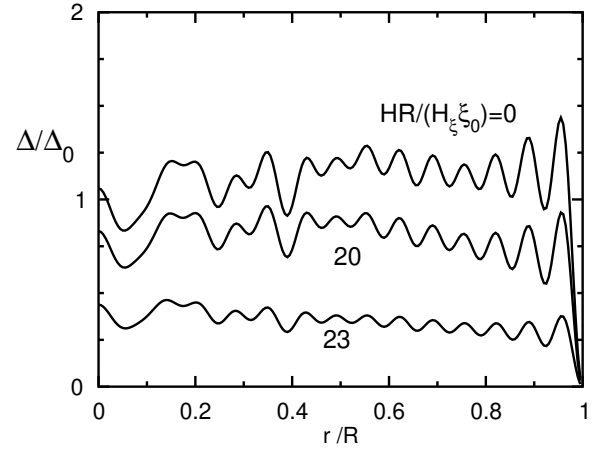


FIG. 4: The order parameter as a function of the radius at small diameter $D = 0 = 0.057$ ($R = 2 \text{ Å}$). The spatial variation of Δ is much stronger than for the large diameter wires of Fig. 3.

B. Small diameters

When the diameter shrinks sufficiently that the transverse level spacings E exceed the order parameter, the density of states on the energy scale of Δ becomes spiky and spatial structure arising from the transverse modes begins to show up in the radial dependence of $\Delta(r)$. Since the level spacing of the transverse modes is inversely proportional to the effective mass ($E = \hbar^2 k^2 / 2m$), the effect of the discrete levels will be strong for systems of small effective mass or low transition temperature. Fig. 4 shows the spatial variation of the order parameter in this regime. A close examination reveals two characteristic length scales in $\Delta(r)$. The shorter length scale (with rapid oscillations) more apparent at large radius) is given in terms of the Fermi velocity, i.e., $r^2 \sim \hbar v_F$. As the Fermi velocity (or the carrier density) grows, $\Delta(r)$ oscillates more rapidly.

Apart from the structures corresponding to the Fermi wavelength, there are more interesting and slowly varying spatial modulations, particularly near $r = 0$. Although these modulations also appear for large diameters (see Fig. 3), their relative importance grows in the smaller diameter wires. This spatial structure arises from the small number of transverse modes within the energy window $[\Delta_D; \Delta_D]$. As can be seen from Eqs. (14, A3), the energy levels close to the Fermi energy contribute strongly to the order parameter. Since the density of states is peaked at the transverse energy levels (see Eq. 16), the resulting order parameter has larger amplitude for the states with $\hbar^2 k_{\perp}^2 / 2m = 2m R^2$, $k_z = 0$ and displays the spatial characteristics of those transverse modes. As illustrated in Fig. 5, the states within the k -space shell of area $2k_F k_z = 4\pi \Delta_D$ contribute most strongly to the order parameter. Although we have used sharp energy cut-offs at Δ_D , they are not expected to impose a significant quantitative change because the weight factor in

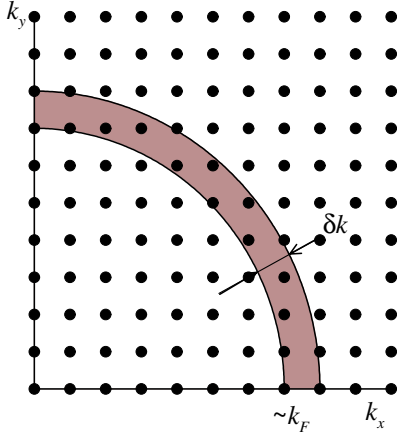


FIG. 5: Schematic 2-dimensional phase space with zero axial wavevector ($k_z = 0$). Transverse modes within the shell of thickness k_F contribute strongly to the order parameter. The area of the shell $2k_F k_F = 4\pi k_F^2$ does not depend on the choice of Fermi energy.

the gap equation, $u/v = 2 \frac{p}{n^2 + \frac{1}{2}}$ (cf. Eq. (A2)), is small near the cutoff. The ratio of u/v for $n = 0$ to $n = \infty$ is approximately $\frac{1}{25}$.

The shape of the order parameter is determined by which states happen to fall into the k -space shell. For instance, if states of $(m = 0)$ are absent in the shell, then the amplitude $\langle r' = 0 \rangle$ is depleted, since only the Bessel functions of J_{0j} have non-vanishing values at $r = 0$. We caution that the order parameter is not necessarily zero at $r = 0$, since there are also states (m, j, k) with finite k . As the diameter decreases, the transverse states become more sparse in the energy shell and the spatial structure becomes more pronounced. In contrast, large-diameter wires have many contributing $(m, j, k = 0)$ states and the spatial variation averages out.

Averaged order parameters at zero magnetic field are plotted as a function of diameter in Fig. 6. The temperature is fixed at 0.2 K and 3 different radial smearings $R = 0; 2; 5$ Å are used. The filled circles are solutions for full BdG equations and the open circles impose the constraint of a constant Δ . Regardless of R and the spatial constraint, Δ/Δ_0 converges to 1 at large diameter. Δ/Δ_0 fluctuates considerably as the diameter decreases, with more scatter for smaller radius smearing. These variations arise from the sharp van Hove singularities in the density of states at transverse eigenvalues. Interestingly, the full BdG order parameter is consistently larger than the constant solution. The gap equation, Eq. (14) or (A3), becomes particularly simple for a constant Δ at $T = 0$,

$$\frac{1}{V} = \sum_{\mathbf{k}} \frac{\Delta}{\epsilon_{\mathbf{k}}^2 + \frac{1}{2}}; \text{ with } \epsilon_{\mathbf{k}} = \sqrt{\mathbf{k}^2 + \frac{1}{2}} \quad (21)$$

where ϵ is the non-interacting eigenvalue (absorbing chemical potential). Although the density of states

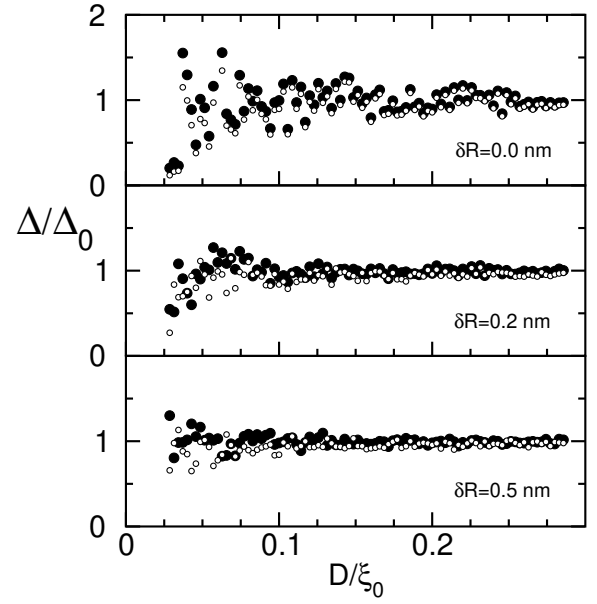


FIG. 6: Average order parameters Δ as a function of diameter for different radius smearings R . Filled circles are the full BdG solution while empty circles represent the constrained case where spatial variation of Δ is disallowed. Concomitant effects appear at $D = 0.05$ Å, i.e., when the transverse energy level spacing E_{\perp} converges to about 4 K as the diameter increases, regardless of R . In the full solution, Δ increases slightly as $D = 0$ drops below about 0.1. Compared to the constant- Δ behavior, this enhanced order parameter takes advantage of the spatial variation in the BdG solution.

$\Delta(D)$ at diameter D has fluctuations due to discrete transverse energy levels, it averages to the bulk limit. Therefore, statistically, Δ is expected to fluctuate about the bulk value Δ_0 . Particular lineshape of the curves (of empty circles) in Fig. 6 is due to limited diameter sampling and the re-tuning of model parameters. As the calculation of $R = 0.5$ nm indicates, stronger broadening suppresses the fluctuation of the order parameter which will converge to Δ_0 down to small D . When the condition of the uniform Δ is relaxed, Δ has the freedom to peak in regions with a higher density of electronic states, thereby increasing the condensation energy. For all R shown here, the enhanced order parameter is most evident for $D = 0$ smaller than about 0.1, the diameter regime where the transverse level spacing becomes comparable to Δ . For $D = 0$ of 0.05–0.1, the enhancement is roughly 10–20%. This is consistent with larger T_c in small samples, as is often observed in thin films^{23,24,25}. This tendency has been attributed to softening of surface phonons in samples of small dimension. The spatial variation of the order parameter from concomitant effects may also contribute to this trend.

The order parameter versus magnetic field plotted in Fig. 7 shows shoulders that also reflect the discrete nature of the transverse modes. The overall shape of the curves is similar to that for large diameters (see

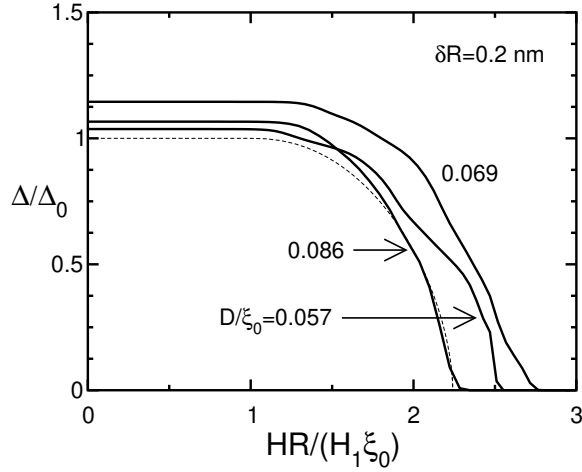


FIG. 7: The order parameter as a function of the external field at a small diameter $D = 0.057$ – 0.086 ($D = 20$ – 30 nm, $R = 2$ Å). displays several shoulders as the field increases and then vanishes abruptly, unlike the large diameter case of Fig. 1. This structure reflects the discrete nature of the transverse modes. The sudden cut-off at the critical field is due to an absence of small angular momentum transverse states near the chemical potential. The dashed line is Eq. (18).

Fig. 1). remains constant until the depairing field e_h in Eq. (A 3) becomes comparable to Δ . As the field increases further, distinctive shoulders appear. As shown in Eq. (A 3), until the condition $\frac{p^2}{2m} + \frac{\hbar^2 k^2}{2m} < e_h$ is satisfied for any non-interacting state, the thermal factor $1 - 2f$ does not change, so the gap equation yields the same Δ . At large diameters, the number of depaired states with $\frac{p^2}{2m} + \frac{\hbar^2 k^2}{2m} > e_h$ increases gradually and therefore varies steadily with the external field H . However, at small diameters, the density of states has peaked structures with van Hove singularities separated by an energy spacing of $\sim \hbar^2 \pi^2 / m R^2$. Since only a few transverse energy peaks are available in the energy window, the van Hove singularities have a stronger influence on the order parameter. Therefore kinks begin to appear in the field dependence of Δ . As D grows, these discrete structures smooth out, as in Fig. 1.

The R -dependence of the critical field H_c is shown in Fig. 8. Electron orbits in more tightly confined spaces are less influenced by magnetic field, because of the smaller depairing contribution ($e = \hbar c / d$) in the phase of wavefunction. The filled circles are BdG solutions with $R = 2$ Å and the dashed line is the semiclassical (i.e. $1=R$) solution of the BCS equation Eq. (19). The inset magnifies the small diameter regime. The BdG solution follows the $1=R$ trends well down to about $D = 0.02$. As D gets smaller, H_c fluctuates substantially, but follows the overall $1=R$ behavior surprisingly well. One of our findings is that the prediction of the Ginzburg-Landau theory agrees remarkably well with the microscopic solution of the BCS equation, down to small diameters ($D = 0$). This conclusion may change with an inclusion

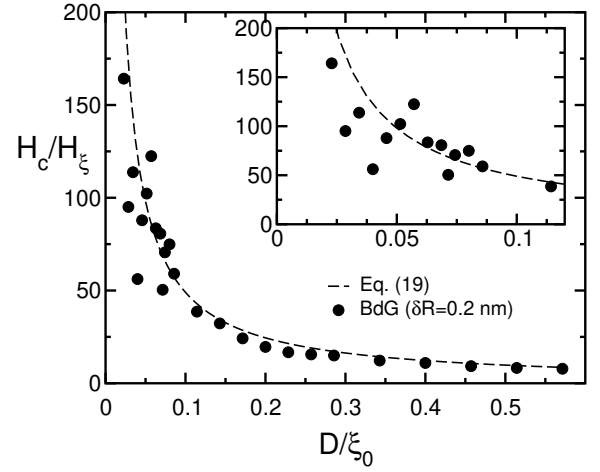


FIG. 8: The critical field vs rod diameter. The critical field H_c varies inversely proportional to the diameter D . The solutions of the full BdG equation follow the general trend of Eq. (19), which was obtained from the BCS equation under the constraint of a spatially constant order parameter. The full BdG solution satisfies the $1=R$ prediction down to fairly small diameters, far smaller than coherence length, although they fluctuate strongly about the relation Eq. (19).

of strong interaction effects, such as increasing Coulomb interaction in strong confinement at small diameters.

Finally, we mention that temperature dependence of the order parameter does not show significant deviation from the BCS results²⁶. The relation $\hbar k_B T_c = 1.764 \Delta$ holds to high accuracy for a wide range of diameters at zero external field.

IV. CONCLUSIONS

We have studied the dynamics of the transverse degrees of freedom in superconducting nanowires. As the confinement dimension shrinks and the level spacing becomes comparable to the order parameter, the discrete nature of the transverse modes shows up in a spatial variation of Δ . In the clean limit, electronic angular momenta are conserved and couple strongly to magnetic field to shift the quasi-particle energy levels. This effect shows up as distinct shoulders in the response to an external field. In a confinement scale comparable to or larger than the superconducting coherence length, superconducting wavefunctions satisfy the usual boundary condition for normal derivative $\partial \Delta / \partial n = 0$ for superconducting order parameter. Under zero magnetic field, Δ remains constant throughout the sample, except for small and rapid oscillations. With finite external field, adjust to the vector potential with much stronger spatial variations than predicted in Ginzburg-Landau theory.

Our results are relevant to clean-limit samples with inclusion of level broadening effects introduced by uncertainties in diameter. It is useful to compare the results with the dirty-limit theories^{7,8,12,16}. Although detailed

mechanisms for both limits are different, both systems display gapless behavior. The critical fields for the disappearance of order parameters, H_c , behave quite differently for the two limits. In the dirty limit¹² ($\xi = 0$), H_c becomes very large (before the spin-Zeeman depairing effect dominates²⁰), with $H_c(\infty) = H_{c0} = \sqrt{H_{c0}^2 + H_{c0}^2}$ with H_{c0} given in Eq. (19) for the clean limit ($\xi = 0$). For the critical field H_1 where the excitation spectrum first becomes gapless, $H_1 = H_{c0} j_1 = 0.954$ while $H_1 = H_{c0} j_1 = 0.389$. Therefore, the clean limit remains gapless for a wide part of the magnetic field range compared to only 4.6% of the dirty limit. While the on-set of the order parameter suppression and the disappearance of the excitation gap happen simultaneously in the clean limit, the closing of the excitation gap in the dirty limit happens only when the superconducting order is already suppressed significantly.

Electrodeposition into nanoporous membranes such as polycarbonate or anodic alumina¹³ can yield single-crystal metallic nanowires from several different superconducting metals (tin, lead, etc.). Such system may be able to access the clean limit in which the phase information of definite angular momentum states is conserved and orbital-derived level-shifts under magnetic field become substantial. Since the effects of discrete levels begin to appear when the level spacing becomes comparable to the order parameter (cf. Eq. (17)), systems of smaller diameter will exhibit stronger confinement effects at a given wire diameter. Systems with small band mass will have similarly strong confinement effects.

The nature of confined superconductivity in single-crystalline metallic nanorods could perhaps be varied most clearly by the gapless spectrum that appears at magnetic fields smaller than the critical field. The small quasi-particle excitation energy here could result in very interesting physics, e.g. in specific heat measurements at temperatures below T_c under external field. Gapless superconductivity under an external field could also enhance phase-slip rates as reflected in the electrical resistivity. Due to the low quasi-particle excitation energies, thermal or quantum fluctuations will overcome the condensation energy more easily. Gapless excitations for normal electrons could contribute to a finite residual resistance in the presence of strong scattering at the confining surface.

Acknowledgments

We thank M. Tian, M. Chan and Y. Liu for very helpful discussions. We acknowledge support from the National Science Foundation DMR-0213623 and the David and Lucile Packard Foundation.

APPENDIX A: SEMI-CLASSICAL SOLUTION FOR ORDER PARAMETER IN CYLINDER

We derive the analytic solution to the gap equation Eq. (14) with the constraint of a uniform order parameter. The relevant regime is when the cylinder is large enough that the transverse level spacing is much smaller than ξ and the external field is not too close to the critical value. Similar results have been derived for spherical system using a Green function technique.¹² With the assumption of a constant Δ , one approximates $[r; p] \approx 0$, treating r and p as independent variables. We ignore the Zeeman term from spins, $\mu_B H$ in Eq. (2), since it is negligible in the regime of interest. The term quadratic in the field, $e^2 A^2 = 2m^* c^2$, is also dropped, as discussed below. Under these conditions, the non-interacting Hamiltonian becomes $H_0 = \sum_k \epsilon_k a_k$, where $\epsilon_k = \frac{1}{2} m^* v^2$ and

$$\epsilon_h = \frac{e}{2m^* c} L H : \quad (A1)$$

Solving the BdG equation Eq. (1) for a constant Δ , one obtains

$$E_k = \sqrt{\epsilon_k^2 + \Delta^2} a_k; \text{ and } u_k v_k = \frac{\Delta}{2 \sqrt{\epsilon_k^2 + \Delta^2}} : \quad (A2)$$

With these approximations, $u_k v_k$ is independent of the field H . The gap equation can be rewritten as

$$1 = V \sum_k \frac{1}{2} \frac{2f(\frac{\epsilon_k^2 + \Delta^2}{2})}{\epsilon_k^2 + \Delta^2} : \quad (A3)$$

The effect of the magnetic field is reflected only in the Fermi-Dirac function f . To evaluate the angular momentum summation, we write $\epsilon_h = (e/2m^* c) L H = (e/2c)(r - v) H = (e/2c)(H - r) v$. Now, with a fixed r and H and an isotropic distribution of v , $\epsilon_h = (ev_F/2c)rH \cos \theta'$ with the angle $\theta' = \angle(H - r; v)$ and $j_y j_z = \frac{1}{2} \epsilon_h$. The summation on the right-hand side of the gap equation Eq. (A3) becomes

$$\sum_{\mathbf{h}} \int_0^R dN_0 \int_0^R \frac{2 dr r}{R^2} \frac{d v}{4} \frac{1}{2} \frac{2f(\frac{\epsilon_h^2 + \Delta^2}{2})}{\epsilon_h^2 + \Delta^2}; \quad (A4)$$

where N_0 is the density of states and \int_v the solid angle for v . If $e^2 A^2 = 2m^* c^2$ is much smaller than the integral limit \int_D , it can be absorbed in the chemical potential with little change in the integral \int_D . The gap equation becomes

$$1 = N_0 V \int_0^R dN_0 \int_0^R \frac{1}{2} \frac{2f(\frac{\epsilon_h^2 + \Delta^2}{2})}{\epsilon_h^2 + \Delta^2} du u \int_1^R \frac{1}{2} \frac{2f(\frac{\epsilon_h^2 + \Delta^2}{2})}{\epsilon_h^2 + \Delta^2} du u; \quad (A5)$$

with $u = r/R$, $\cos \theta' = u$ and $h = (ev_F/2c)RH$. For $H = 0$, we have

$$1 = N_0 V \int_0^R dN_0 \int_0^R \frac{1}{2} \frac{2f(\frac{\epsilon_h^2 + \Delta^2}{2})}{\epsilon_h^2 + \Delta^2} du u \int_0^1 \frac{1}{2} \frac{2f(\frac{\epsilon_h^2 + \Delta^2}{2})}{\epsilon_h^2 + \Delta^2} du u : \quad (A6)$$

Since $f = 0$ for $\frac{p}{\hbar^2 + \frac{1}{2}} > \hbar u$ in the $T = 0$ limit, we can perform the integral in Eq. (A5)

$$\begin{aligned} & \int_0^{\frac{p}{\hbar^2 + \frac{1}{2}}} \frac{1}{u} du = \ln \left(\frac{p}{\hbar^2 + \frac{1}{2}} \right) \\ & = \frac{1}{2} \ln \left(1 + \frac{1}{2} \right) + \frac{1}{2} \ln \left(\frac{p}{\hbar^2} \right) \end{aligned}$$

for $\hbar = \hbar_0 > 1$, and 0 for $\hbar < 1$. For $\hbar > 1$, Eq. (A5) becomes

$$\begin{aligned} 1 &= N_0 V \ln \left(\frac{p}{\hbar^2 + \frac{1}{2}} \right) \\ &+ \frac{1}{2} \ln \left(1 + \frac{1}{2} \right) + \frac{1}{2} \ln \left(\frac{p}{\hbar^2} \right) \end{aligned} \quad (\text{A7})$$

Subtracting Eq. (A6) from Eq. (A7) and using \hbar_D , we obtain Eq. (18). The order parameter becomes gapless as one or both of the states in the time-reversed pairs in Eq. (A2) are pushed out of the Debye frequency. The external field induces T_c by the statistical factor, not directly through the field dependency in the non-interacting density of states, as can be inferred from Eq. (A5). The density of states over the interaction window of the Debye frequency remains nearly the same due to a balance between the out flux and the in flux of non-interacting energy levels shifted by the external field.

APPENDIX B: GINZBURG-LANDAU THEORY

Here we consider only a stationary superconducting order parameter ($L_z = 0; k_z = 0$) where the Ginzburg-Landau functional for the order parameter reads

$$\begin{aligned} F &= \int d^3r \left[\frac{1}{2} |\nabla \psi|^2 + \frac{1}{2} \mu_0^{-1} |\mathbf{A}|^2 \right. \\ &\left. + \frac{H_c^2}{8} \psi^2 + \frac{1}{2} \mu_0^{-1} |\mathbf{A}|^2 \right] \end{aligned} \quad (\text{B1})$$

$$= \frac{H_c^2}{8} \int d^3r \psi^2 + \frac{1}{2} \mu_0^{-1} \int d^3r |\mathbf{A}|^2 \quad (\text{B2})$$

H_c is the bulk critical field, $\mu_0 = 4\pi \times 10^{-7} \text{ T m/A}$ is the permeability of free space, and \hbar is the coherence length. The Coulomb gauge is used for the vector potential $\mathbf{A} = \frac{1}{2} r \hat{\mathbf{r}}$. For radius R much smaller than the penetration depth, the screening of external fields is negligible, as assumed in the main text. With constant f , we obtain the average free energy after integration over the cylindrical nanowire,

$$F = \frac{H_c^2}{8} \pi R^2 \int_0^R r dr \left[1 + \frac{1}{2} \left(\frac{m_0 \hbar c R}{\hbar^2} \right)^2 f^2 + \frac{1}{2} f^4 \right] \quad (\text{B3})$$

We have also numerically minimized the free energy with a spatially varying f , but the spatial variation was far less significant (about 1 percent of the average order parameter for $R = 0.5$) than that of the Bogoliubov-de Gennes results discussed in the text. Therefore, the following approximate value for the critical field is quite accurate. Minimizing Eq. (B3) over f gives

$$f = 1 - \frac{1}{2} \left(\frac{m_0 \hbar c R}{\hbar^2} \right)^2 \quad (\text{B4})$$

For vanishing f , the critical field is

$$H_c = \frac{H_c^2}{R} = 0.450 \frac{H_c^2}{R} \quad (\text{B5})$$

with $\hbar_0 = \hbar c / 2e$.

¹ E. C. Stoner and E. P. Wohlfarth, *Philos. Trans. R. Soc. London, Ser. A* 240, 599 (1948).

² D. V. Averin and K. K. Likharev, *J. Low Temp. Phys.* 62, 345 (1986).

³ "Molecular Electronics: Science and Technology", eds. A. Aviram and M. Ratner, *Annals of the New York Academy of Sciences* 852, New York (1998).

⁴ S. John, *Phys. Rev. Lett.* 58, 2486 (1987); E. Yablonovitch, *Phys. Rev. Lett.* 58, 2059 (1987).

⁵ J. M. Graybeal, P. M. Mankiewich, R. C. Dynes and M. R. Beasley, *Phys. Rev. Lett.* 59, 2697 (1987).

⁶ D. C. Ralph, C. T. Black and M. Tinkham, *Phys. Rev. Lett.* 78, 4087 (1997).

⁷ M. Tinkham, *Introduction to Superconductivity*, Krieger Publishing Company (1975).

⁸ P. G. de Gennes, *Superconductivity of Metals and Alloys*, Addison-Wesley Publishing Company (1989).

⁹ H. Suderow, E. Bascones, A. Izquierdo, F. Guinea and S. Vieira, *Phys. Rev. B* 65, 100519 (2002).

¹⁰ V. R. Misko, V. M. Fomin and J. T. Devreese, *Phys. Rev. B* 64, 014517 (2001).

¹¹ K. Maki, "Superconductivity" Vol. II, Chapter 18, R. D. Parks (ed.), Marcel Dekker, New York (1969).

¹² S. Strassler and P. Wyder, *Phys. Rev.* 158, 319 (1967).

¹³ M. Tian, J. Wang, J. Snyder, J. Kurtz, Y. Liu, P. Schier, T. E. Mallouk and M. H. W. Chan, submitted to *Appl. Phys. Lett.*

¹⁴ N. Giordano, *Phys. Rev. B* 41, 6350 (1990).

¹⁵ A. Bezryadin, C. N. Lau and M. Tinkham, *Nature* 404, 971 (2000).

- ¹⁶ M. Kato and K. Maki, *J. Magn. Magn. Mater.* 226, 280 (2001).
- ¹⁷ Inclusion of finite angular momentum ($L_z = \hbar m$) components in the BdG equation produced far smaller amplitudes than the zero angular momentum component. See also Ref.¹⁰.
- ¹⁸ L. Larkin, *Zh. Eksperim. i Teor. Fiz.* 48, 232 (1965) [English transl.: *Soviet Phys.-JETP* 21, 153 (1965)].
- ¹⁹ Eq. (19) gives a steeper drop of ψ_0 as $\hbar_c \rightarrow \hbar_c^*$ ($\hbar_c^* = 2\hbar_c \ln(\hbar_c/\hbar_0)$) than typical $\psi_0 = \frac{\hbar}{1 - \hbar^2/\hbar_c^2}$ ($\hbar_c = 2.24 \hbar_0$).
- ²⁰ P. Fulde, *Adv. Phys.* 22, 667 (1973).
- ²¹ If the commutation relation between position and momentum is ignored,^{12,18} we always have $\psi(r=0) = \psi_0$ at arbitrary field since the vector potential is zero.
- ²² For the curve of $H_R = (H_0) = 2.16$ in Fig. 3, $j(r)j^2$ decays nearly by a factor of 7 at $r = R$.
- ²³ M. Strongin, O. F. Kammerer, J. E. Crow, R. D. Parks, D. H. Douglass Jr. and M. A. Jensen, *Phys. Rev. Lett.* 21, 1320 (1968).
- ²⁴ J. M. Dickey and A. Paskin, *Phys. Rev. Lett.* 21 1441 (1968).
- ²⁵ H. M. Jaeger, D. B. Haviland, B. G. Orr and A. M. Goldman, *Phys. Rev. B* 40, 182 (1989).
- ²⁶ J. Bardeen, *Rev. Mod. Phys.* 34, 667 (1962).